ISSN: 2182-2069 / E-ISSN: 2182-2077

Enhancing Lung Cancer Classification using CT Images using Processing Techniques Employing U-Net Architecture

Mohammed S. H. Al-Tamimi[1*], Saadya Fahad Jabbar[2], Ahmed Majid Taha[3], and Farah khiled AL-Jibory[4]

[1*]Computer Science Department, College of Science, University of Baghdad, Baghdad, Iraq. mohammed.s@sc.uobaghdad.edu.iq, https://orcid.org/0000-0002-6005-1964

[2]College of Education – IBN Rushed for Human Science, University of Baghdad, Baghdad, Iraq. saadya.fahad@ircoedu.uobaghdad.edu.iq, https://orcid.org/0000-0002-9871-3724

[3] College of Biomedical Informatics, University of Information Technology and Communications, Baghdad, Iraq. dr.ahmed_majid@uoitc.edu.iq, https://orcid.org/0000-0003-4823-1599

[4] Ministry of Education, Karkh First Directorate of Education, Baghdad, Iraq. csd1b0037@gmail.com, https://orcid.org/0009-0000-4290-9376

Received: February 17, 2025; Revised: March 29, 2025; Accepted: May 08, 2025; Published: May 30, 2025

Abstract

There is a consensus that accurate and timely diagnosis of lung cancer is crucial, and it is considered a serious condition, essential for effective treatment of affected individuals. Conversely, several previous studies have examined issues related to automated AI-based systems involving diagnostic results, aiming to diminish the difficulties related to human observation by integrating computer-aided diagnosis (CAD) systems into the diagnostic workflow to enhance efficiency and improve outcomes. This paper discusses the impact of image processing techniques on automated lung cancer detection using computed tomography (CT) scan images and demonstrates their key role in improving model performance. A pre-trained U-Net model was used in conjunction with a set of Gaussian difference (DoG) filters and a CLAHE filter. A detailed examination of a publicly available CT dataset from the Iraqi Teaching Oncology Hospital/National Cancer Center (IQ-OTH/NCCD) included careful comparisons regarding the training efficiency between image processing and non-processing methods. The results achieved were of high quality and satisfactory with the proposed methodology. The results with processing achieved an accuracy of 99.8%, a precision of 99.5%, and F1 score of 99.8%, while without processing, it achieved an accuracy of 97.1%, a precision of 95.2%, and F1 score of 96.11%. These results demonstrate the potential to advance personalized medical imaging and life-saving care.

Keywords: CT, Data, Processing, Lung, U-Net model, Clahe, Gaussian.

1 Introduction

Cancer is among the most lethal diseases impacting people. Lung cancer is the most prevalent kind and the primary cause of cancer-related mortality globally Raghuram (2024). Nevertheless, its intricate pathophysiology and varied cellular architecture impede early detection and intervention. Non-small cell

Journal of Internet Services and Information Security (JISIS), volume: 15, number: 2 (May), pp. 590-609.
DOI: *10.58346/JISIS.2025.I2.041*

*Corresponding author: Computer Science Department, College of Science, University of Baghdad, Baghdad, Iraq.

lung cancer (NSCLC) and small cell lung cancer (SCLC) exhibit diverse biological traits, treatment responses, and prognostic outcomes (Zhang et al., 2019). As a result of these cells and their nature, the inaccuracy or difficulty in classifying cancer, especially early-stage lung cancer, increases the complexity of the complex pathology, hindering early detection and treatment Al Jibory, Mohammed & Al Tamimi (2022). Non-small cell lung cancer (NSCLC), comprising 85% of lung cancer instances, progresses gradually and encompasses various subtypes, such as adenocarcinoma, squamous cell carcinoma, and large cell carcinoma (Wang, 2022). Small cell lung cancer, comprising 15% of lung cancer cases, has rapid growth and early metastasis, rendering it more dangerous khiled AL-Jibory, Younis & Al-Tamimi (2022). The discrepancy in biological behavior influences therapy alternatives and prognosis, requiring accurate classification for successful management Dodia, Annappa & Mahesh (2022). Lung cancer resulted in approximately 1.8 million fatalities globally in 2020, highlighting the necessity for improved diagnostic and therapeutic measures. Effective lung cancer treatment necessitates a comprehensive understanding of its pathological intricacies and tailored therapeutic protocols grounded in precise disease staging Suresha & Devika (2022). The staging of lung cancer by advanced image processing has transformed diagnosis by improving image classification accuracy, precision, and recall (Majumder et al., 2024). These techniques employ advanced filters to examine lung images at several scales, capturing both macroscopic structures and tiny details essential for precise cancer staging. This assists machine learning and deep learning in pinpointing areas of interest in pulmonary imaging (Al-Husseini & Sajit, 2021). Interpretability assists radiologists and oncologists in assessing and trusting automated diagnostic recommendations, hence facilitating more informed decision-making. The newly developed approaches establish a strong and dependable system that addresses picture fluctuation and data imbalance, hence providing consistent and accurate lung cancer diagnosis (Dodiya et al., 2022). This research employs a lung cancer dataset and deep learning to demonstrate the influence of image processing on the efficacy of the suggested method (Krishnaiah & Dayanand Lal, 2025).

2 Medical Image Types

Medical imaging modalities have revolutionised healthcare diagnostics by providing a variety of techniques for different medical demands (khiled AL-Jibory et al., 2022). X-ray, CT, MRI, and ultrasound represent the most common imaging modalities, each with its own benefits and uses that aid in diagnosis (Al-Tamimi & Sulong, 2014). MRI gives excellent soft tissue information, making it useful for identifying neurological and musculoskeletal diseases, while X-ray imaging is best for bone fractures and lung conditions (Al Jibory et al., 2022). The imaging technique depends on the suspected medical problem, the anatomical area of interest, and the clinical decision-making information needed. Imaging innovations like the switch from 2D film to 3D and 4D digital mammography have improved diagnostic accuracy and depth AL-Huseiny & Sajit (2021). Medical imaging technology changes constantly; therefore, practitioners must continue to learn and adapt to optimize patient outcomes (Al-Tamimi et al., 2015). This evolving medical imaging environment emphasizes the significance of choosing the right modality for each clinical circumstance to improve diagnostic precision and treatment planning Sharma & Iyer (2023). Table 1 summarizing the differences in common medical images used to diagnose lung illnesses Kumar et al. (2024).

Table 1: Summarized differences in types of medical images

Type	Description	Image
X-RAY (Chen et al., 2020)	X-rays are electromagnetic energy like visible light. Their advantages: Because they have more energy than light, X-rays can penetrate most objects, including biological things. Medical X-rays show body tissues and structures. An X-ray detector on the patient's other side captures "shadows" of body things.	
CT SCAN (Qadir et al., 2024)	A computed tomography (CT) scan creates detailed bodily images using x-rays. The computer makes cross-sectional slices of bones, blood arteries, and soft tissues in many sections from very small to extremely large, from the beginning to the end of the body. CT scans show more information than x-rays. They can detect sickness or injury and plan medicinal, surgical, or radiation treatment.	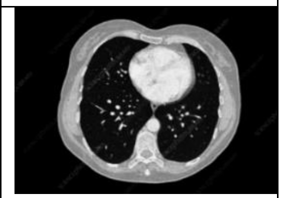
MRI (Kalavathi & Prasath, 2016)	Magnetic fields and radio waves are used in MRI to see body parts. Herniated discs and damaged ligaments are diagnosed with them. The most expensive imaging is MRI. They can illustrate delicate body systems and tissues with sophistication. Imaging with MRI can detect brain tumors, spinal cord damage, and other diseases.	
Ultra sound (Gayathri et al., 2023)	Ultrasound, also known as sonography, visualizes the internal structures of the body, i.e., the internal organs. These images help diagnose and treat many diseases and conditions, but they are limited to the external appearance or movement of organs, and the internal contents cannot be clearly analyzed. Therefore, they are most commonly used to detect fetuses.	
Nuclear (Seibert & Boone, 2005)	Nuclear medicine images the body using radioactive tracers. It is often used to diagnose cancer, heart disease, and other diseases. Radioactive tracers are used in nuclear medicine to image the body.Intravenous tracers are absorbed by targeted tissues. Tracer radiation is observable using a particular camera. Nuclear medicine is used to diagnose cancer, cardiovascular disease, and other diseases.	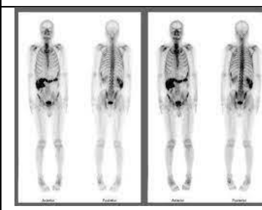

3 Related Work

Of the various studies using the IQ-OTHNCCD lung cancer dataset, these are the most significant:

- **Kareem et al., 2021:** Development/analysis of a lung cancer dataset, an image processing/computer vision system is presented to detect lung cancer in the dataset. There are three pre-processing steps: picture enhancement, segmentation, and feature extraction. The final stage uses SVM to classify slides as normal, benign, or malignant. Different SVM kernels and feature extraction methods are tested.
- **AL-Huseiny & Sajit, 2021:** Computer algorithms have grown widely used for specialized help and early diagnosis. In order to identify lung CT images containing malignant nodes, this study suggests applying Deep Neural Networks (DNN). In order to extract the targeted regions, the area of lungs, and eliminate adjacent tissues and artifacts, the method uses quick and easy pre-processing of input pictures. Images are centered, and their sizes adjusted prior to training and validation in a deep neural network. This study reads only GoogLeNet DNN for medical data using transfer learning Aulakh et al. (2025). This constrains deep layers while allowing the DNN's last layers to evolve. For an incomplete product

- **Suresha et al., 2022:** The proposed approach in this study demonstrates that combining the pre-trained EfficientNetB7 model with new features, combining deep and statistical features, can avoid the data imbalance problem in the dataset. The balanced feature set becomes more consistent through these generated features. Classification is performed using the SVM classifier, which is the most commonly utilized in machine learning. Experimental studies on the lung cancer dataset show that the performance of our suggested method is better compared to conventional techniques. This experimental study shows that the proposed model is effective in measuring.
- **Qadir et al., 2024:** The Hybrid Lung Cancer Staging Classifier and Diagnostic Model (Hybrid-LCSCDM) detects lung cancer. The approach streamlines lung cancer diagnosis by classifying patients as normal, benign, or malignant. It analyzes CT scans in two steps: Initial feature extraction uses a pre-trained model called VGG-16 to identify cancer-related lung CT scan features. It then uses XGBoost to classify scans into three categories using these features. To prove its efficacy, the model was examined and assessed on Lung Cancer. The dataset comprises 1190 photos from the three categories above.
- **Gulsoy & Kablan, 2024:** introduce FocalNeXt, a vision transformer-based model that automates lung cancer diagnosis in CT images using the best characteristics of ConvNeXt and FocalNet. Combined with the vision transformer model, where ConvNeXt extracts and FocalNet enriches data under a self-attention process, this hybrid two-stem design may improve diagnostic accuracy Bhardwaj & Ramesh (2024). A detailed examination of the publicly accessible dataset includes comparisons and an ablation study. With over 98% accuracy, FocalNeXt delivers cutting-edge results. FocalNeXt's ablation study shows its efficacy and versatility, highlighting its potential to improve medical imaging and tailored healthcare.
- **Majumder et al., 2024:** Researchers present the Mitscherlich function-based Ensemble Network (MENet), an ensemble model for improving lung cancer prediction accuracy. MENet takes into account the prediction probabilities obtained from three deep learning models: Xception, InceptionResNetV2, and MobileNetV2. The Mitscherlich function generates a fuzzy rank to combine the results of the aforementioned basis classifiers; this rank forms the basis of the ensemble method. The lung cancer CT scan datasets used to train and test the proposed method are LIDC-IDRI and Diseases (IQ-OTH/NCCD). The study is summarized in Table 2.

Table 2: Summarized the related work

Re.& year	Method	Dataset	Limitation	Result
2020 (Kareem et al., 2021)	Filter Segmentation svm	(IQ-OTH/NCCD)	Data split technique is not explained only mention the set of training 70% and test 30% and not mention to the value of validation	accuracy 89.88%
2021 (AL-Huseiny & Sajit, 2021)	Roi GoogLeNet DNN	(IQ-OTH/NCCD)	A computationally affordable preprocessing approach is proposed to extract the lung region and remove clutter and extraneous surrounds by multiplying the lung mask by the original image. Calculate the lung bounding box. Finally, photos are normalized. Because this dataset required mentioning the ROI methodology, this procedure was done manually. The CT data moves the lung position in the image, which is an automatic (the shape is small and then larger) sign that the ROI method is accurate. The outcomes were not specified as training or testing.	**Sensitive** 95.08% **Specificity** 93.7% **Accurse** 94.38%

2022 (Suresha et al., 2022)	EfficientNetB7 and Machine Learning are used to create feature fusion. PCA reduces these eEfficnetNetB7 characteristics.	(IQ-OTH/NCCD)	The proposed approach highlights the extraction of features through a pre-trained model and feeding them into the machine learning algorithm. Principal component analysis reduces efficientNet characteristics. This is a very lengthy process as it was possible to use pca with svm and know the results and then apply efficientNet alone as a pre-trained model and know the results and then compare the proposed approach with the two methods mentioned. Also, the type of svm algorithm used was not highlighted and the mechanism for dividing the data was not explained. Only its results were presented. The size of the validation set was not mentioned and the results were not shown. The confusion matrix values results were not shown	**Precision** 98.4% **Recall** 97% **F-score** 97.7%
2024 (Qadir et al., 2024)	Hybrid-LCSCDM) VGG16 for feature extraction and an XGBoost classifier	(IQ-OTH/NCCD)	The classification process involves feature extraction using a pre-trained model, VGG16, preceded by classification of CT images using the XGBoost algorithm. The pre-trained model could have been applied to the unit to see if the approach was improving or not. Also, the data partitioning process was not explained in terms of method and values in addition. Not mention to value of of confusion matrix's value but mention the result of scale only	**Precision** 0.9863 **Recall** 0.9635 **F-score** 0.9736 **Accuracy** 98.54%
2024 (Gulsoy & Kablan, 2024)	FocalNeXt Augmentation	(IQ-OTH/NCCD)	Not mention to value of confusion matrix's value but mention the result of scale only. the split dataset not mention the technical but mention the percentage of split only that mean may be split manual or out	**Without augmentation** **Sensitivity** (99.78%) **F1-score** (99.56%) **Accuracy** (99.81%) **With augmentation** **Sensitivity** (99.78%) **F1-score** (99.56%) **Accuracy** (98.05%)
2024 (Majumder et al., 2024)	MENet (from Xception, InceptionResNetV2, and MobileNetV2 transfer learning-based CNN models)	(IQ-OTH/NCCD) & LIDC-IDRI	Due to the significant evolution of medical data sets, the model's ability to adapt to new information and the potential deviation of concepts remains unclear. This contradicts the idea of research that aims to create a system that supports the doctor, i.e. the system's results were achieved on this data only and a software display mechanism was adopted. This contradicts the mechanism of the scientific paper's writers.	**Recall** **92.9%** **F-score** **92.5%** **Accuracy** 95.7%

4 The Proposed System

Diagnosing lung tumors has become one of the most important topics for researchers, especially recently, as we notice in the following figure 1.the prevalence of lung cancer:

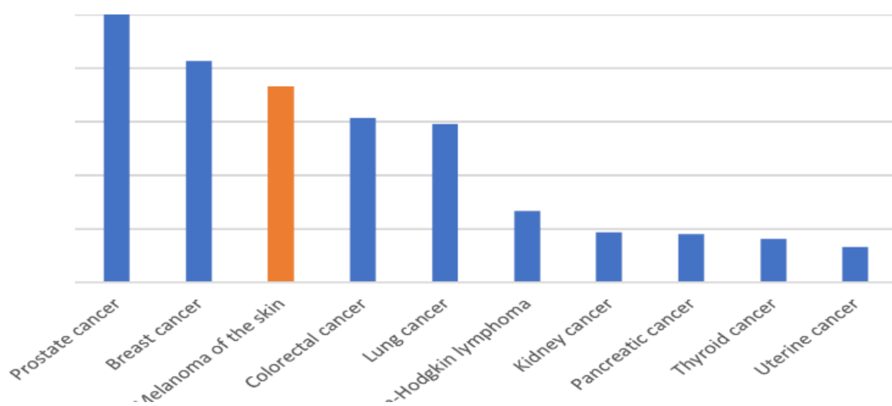

Figure 1: Cancer Incidence to 2024

Based on this statistical diagram that shows the importance and high incidence rates of lung cancer and its spread, the proposed approach was based on the idea of highlighting the importance of initial processing images in enhancing the efficiency of training of the pre-trained model, where Gaussian (Dog) filters were chosen to highlight the borders of the lung and also the Clahe filter to balance the color distribution Aulakh et al. (2025). The output of these filters will be the input to the pre-trained model u-net, which was chosen based on its good working mechanism that is highly efficient and has fewer layers Chen et al. (2020). A comprehensive evaluation of the publicly available CT dataset from the Iraqi Teaching Oncology Hospital / National Cancer Center (IQ-OTH / NCCD) was conducted in the proposed approach. The figure 2 is the general structure of the proposed approach.

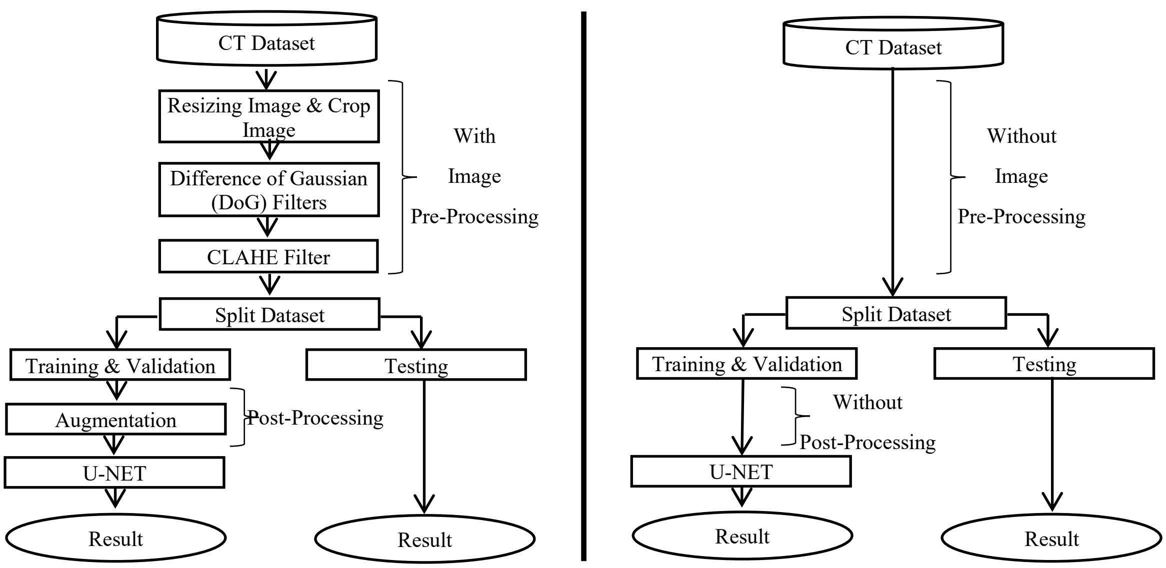

Figure 2: Proposed System Diagram

5 Dataset and Pre-Processing in Proposed System

The lung cancer dataset from the Iraqi Teaching Hospital/National Cancer Center (IQ-OTH/NCCD) was compiled at the Specialized Hospital over a three-month period in autumn 2019. It comprises CT scans of lung cancer patients at different stages and healthy individuals of varying ages. Oncologists and radiologists from both centers diagnosed IQ-OTH/NCCD slices. The dataset comprises 1,190 CT scan slices from 110 individuals, categorized as normal, benign, or malignant. There were 40 cancer cases, 15 benign cases, and 55 normal cases. DICOM CT scans were initially acquired. A Siemens SOMATOM scanner was utilized. CT scanning employed 120 kV, 1 mm slice thickness, a window width of 350–1200 HU, and a reading window center of 50–600 HU. Employing complete breath-hold inhalation. All photographs were anonymized prior to analysis. Regulators exempted written informed consent. The ethical committees of the collaborating medical centers approved the study. All scans were aggregated. Each of these 80–200 layers captured images of the breast from various angles and viewpoints. The 110 participants differed in gender, age, education, region, and lifestyle. Some individuals were engaged as farmers and workers, while others were employed by the Iraqi Ministry of Transport and Oil. The majority originated from central Iraq, encompassing Baghdad, Wasit, Diyala, Salah ad-Din, and Babil. Figure 3 illustrates one example. The description about the dataset is described in table 3.

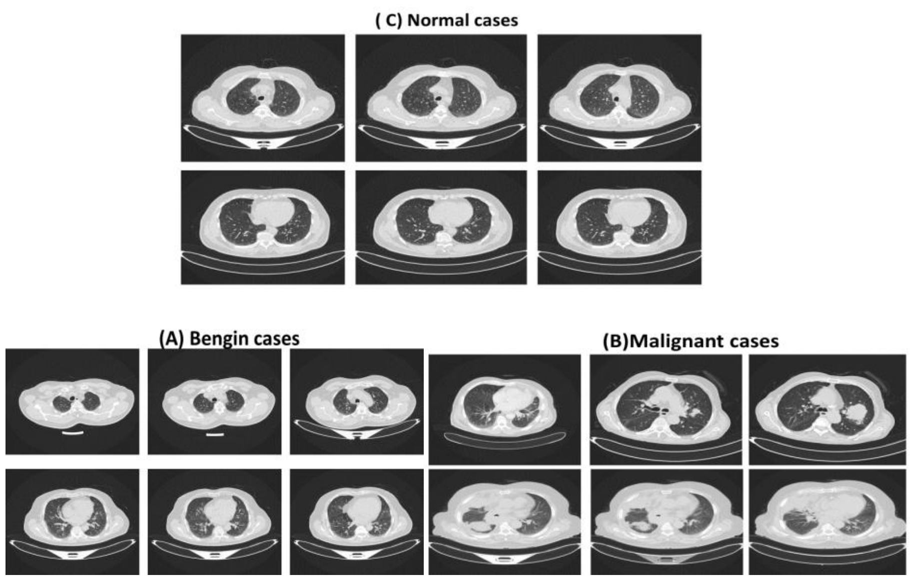

Figure 3: Sample from Dataset

Table 3: Description of Dataset

Description	Description
Purpose	CT scan dataset for lung cancer detection and classification model research.
Source	Iraqi hospitals, OTHNCCD (Oncology and Therapeutic Hospital of Northern CCD).
Content	CT scan images of patients diagnosed with lung cancer in various stages, as well as healthy subjects.
Images	CT chest slices showing different angles and sides.
Cases	110 cases, including: Normal: 55 cases Benign: 15 cases Malignant: 40 cases
Image Count	Approximately 1190 images.
Annotations	Lung cancer status and stage are labeled on each photograph.

Basically resizing and cropping do this. Resizing CT images enhances image quality and standardizes size for case-study consistency. Meanwhile, cropping lets clinicians focus on specific areas of concern, protecting vital anatomical features. The suggested approach resizes the image to 256 × 256 × 3. Based on previous study and scientific experience, this size was chosen. Cropping removes undesired image elements. This procedure reduces extraneous elements and focuses on the lung, making it crucial. Image resolution and clarity are crucial for proper diagnosis and treatment planning in medical imaging, especially lung cancer. A dual filter is utilized after this process. One sophisticated CT image quality improvement method is the difference graph (DoG) filter. The DoG filter removes background noise and highlights important features in images. The DoG filter approximates a Laplacian or Gaussian function, which highlights points of fast light intensity change to capture edges and outlines. By removing an image from a Gaussian-warped version, it isolates areas with high light intensity changes. The DoG filter is more advanced than Gaussian distortion or median filtering. Instead of removing noise across the image like a Gaussian filter, the DoG filter focuses on specific regions to preserve critical details. See Figure 4 for how this filter affects a dataset image. Advances in imaging have transformed medical diagnostics, notably lung cancer detection. In image processing, filters improve image quality and accurately classify medical images. In recent years, the Difference Gaussian filter became popular. It's important to grasp Gaussian filters before learning about the DoG filter. Gaussian filters have a bell-shaped curve for the standard deviation, which affects function spread. This filter reduces noise and blurs features by smoothing photos. However, difference Gaussian filters work more complicatedly. DoG filters increase edge identification by removing an image from a Gaussian-distorted image with two standard deviations. The DoG filter highlights rapid intensity fluctuations to identify structural boundaries in medical pictures. The DoG filter reduces noise and detects edges, unlike Laplace or median filters. It excels at complex medical images that require accuracy. This combination of activities shows the DoG filter's effectiveness in preparing medical images for analysis, especially in lung cancer staging, where correct tumor-tissue relationships are critical.

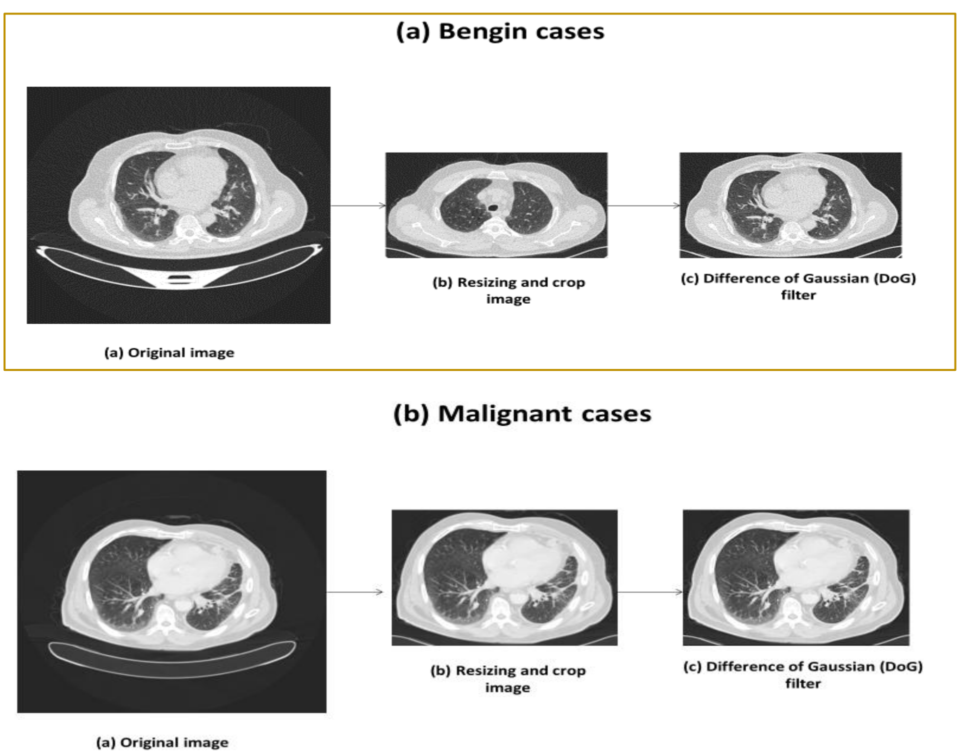

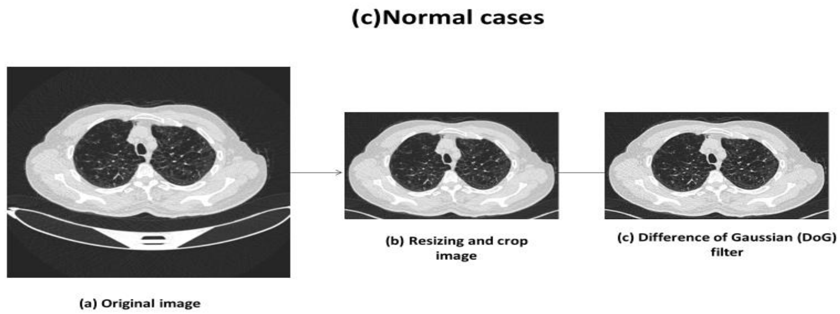

Figure 4: Three Operation Image Processing (Resizing, Crop, DOG filter) in Three Cases.

CLAE is an Adaptive Histogram Equalization mechanism that suppresses Contrast Limited AHE over-amplification. CLAHE is done by finding the histogram inverse in small patches termed tiles and not in the whole image. The neighboring tiles get bilinearly interpolated to remove the artificial discontinuities. It can be applied to optimize the contrast of the image depending on below mentioned parameters (Al-Tamimi & AL-Khafaji, 2022):

- **Block size –** represents the local region surrounding a pixel that undergoes histogram equalization, which is usually greater than the features to be kept.
- **Histogram –** represents the number of bins utilized for histogram equalization. This is actually meaningless since byte resolution is used internally by the implementation. Nevertheless, this will also restrict the output's quantification when processing 24-bit RGB or 8-bit greyscale photos. However, the histogram's bin count ought to be less than the block's pixel count.
- **Max slope -** Limit the stretch of contrast in the function of intensity transfer. An example of a minimax scan above is maximal local contrast. A value of 1 will deliver the input image.
- **Mask -** Any of the images presently open by you can be taken for a mask. The selections and masks are likely mutually exclusive, or else may apply both simultaneously.
- **Process as composite -** Both modalities are capable of processing photos that have numerous color channels.
- **Checked -** estimate the transfer using the image that is shown, and then apply it to each channel separately. Local contrast compression is the preferred option for color images. with more dynamic range and bit depth than is suitable for digital displays.
- **Unchecked -** use the selected channel to process individually.

In short, it is a filter or algorithm that works to balance the contrast of images, that is, it works. It lightens the dark area and darkens the light area, and it is based on the concept of Clip Limit Parameter (CLP). Is denoted by equation 1 (Setiawan et al., 2013)

$$\mathrm{CLP} = \left[\frac{w}{256}\right] + \left[\beta.\left(w - \frac{w}{256}\right)\right] \ldots\ldots\ldots (1)$$

Where:

w Denotes the size of the tile or window area that has to be considered, β is the pre-defined CL

This method is an improvement over the traditional adaptive histogram equalization (AHE) technique, because it effectively mitigates the problem of excessive noise amplification and artifacts that can arise with AHE (Al-Khafaji & Al-Tamimi, 2022).The following point description the steps of CLAHE filter work that lead to use in proposed system.

- Split the image up into tiny, non-overlapping tiles: The image is split up into a grid individual tiles, each representing a local area.
- Determine the histogram for every tile: Every tile's histogram is computed representing the distribution of intensity values within that specific area.
- Apply histogram equalization to each tile: Each tile's histogram is equalized using a traditional histogram equalization method. This stretches the intensity values to fill the full range, enhancing local contrast.
- Limit the contrast amplification: In CLAHE, a clipping process is applied to the equalized histogram to limit the maximum intensity value. This prevents the over-amplification of noise and artifacts.
- Combine the tiles back into the final image: The processed tiles are then combined back together to form the final enhanced image.

Figure 5 shows the effected of filter CLAHE in proposed system.

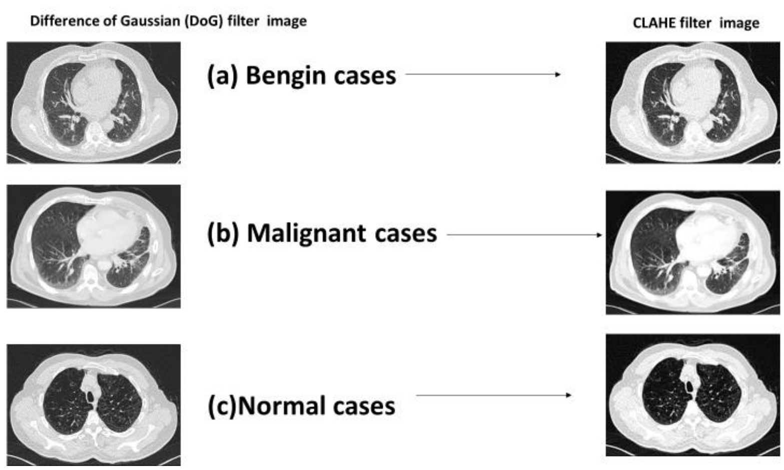

Figure 5: Three Examples of Applying CLAHE filter on the Result of DOG Filter in Three Cases.

The idea of using this type of filter is to create a balance for grayscale images, so it helps to lighten the dark ranges and makes the light ranges darken in a balanced way. After performing the initial data preparation operations, the division process of the data into test and training sets will take place. This will be done based on the k-fold technique, with five experiments. This method was adopted because the division is more accurate and proportionate to the size of the database.

6 Split Dataset and Post- Image Processing

Keeping with the technological approach of the proposed system, the dataset is partitioned into three categories: training, testing, and validation. Out of these, 80% is allocated to testing, while 20% is for training. The data set in the proposed system's training, testing, and verification ratios is reviewed in Table 4 and Figure 6.

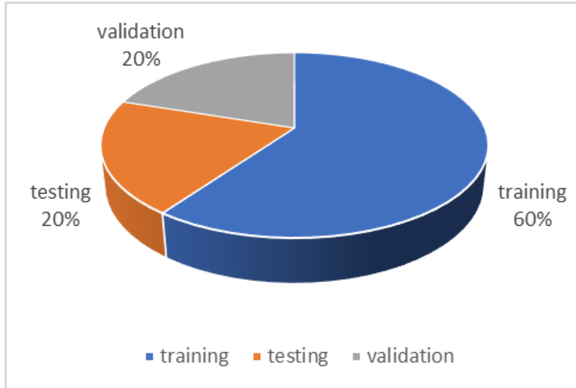

Figure 6: Splitting Dataset as 80% training and 20% testing.

Table 4: Partitioning the dataset in the proposed approach.

Training	60%=762
Testing	20%=238
validation	20%=190

After dividing the data, the data portion allocated for training before the images enter the model is subjected to augmentation operations, the purpose of which is to generate virtual data to train the system on non-existent cases that may affect the system, as shown in the following figure 7.

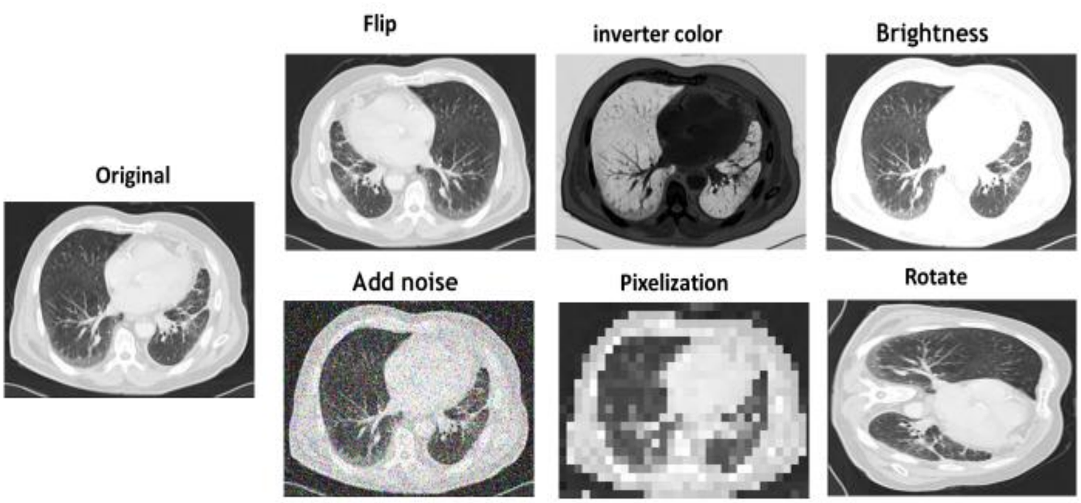

Figure 7: Augmentation Operations in Proposed System

7 Training Stage in Proposed System

The U-Net model, which is the basis for the formation of traditional networks utilized for image segmentation in biomedical, is based on a common deep learning architecture (figure 8). The architecture of this model was designed to address the scarcity of medical data. A large volume of data is treated by the network model effectively with little data, speed, and high accuracy. U-Net has an architecture with contracting and expanding paths. The decoder layers in the expanding path build up the final segmentation map with features encoded at various resolutions at different receptive fields in the network, and are extracted as input at each layer in the contracting path. Meaning at higher layers in the contracting path, where an increasing amount of contextual information, specifying the locations in the image where relevant features go, is drawn from U-Net's contracting path. It encodes information by reducing the image resolution through decreasing spatial information towards higher layers in the model. The contracting path is essentially made up of convolutional neural network layers that look like feed-forward layers, in contrast to which the expanding path decodes information and is used for localization at each layer while keeping the input spatial resolution. Upsampling and convolution of the feature map are done by increasing the path decoder layers. Skip connections from the contracting path in maintaining lost spatial information helps the path to decode, aiding the localization of features for the decoder layers.

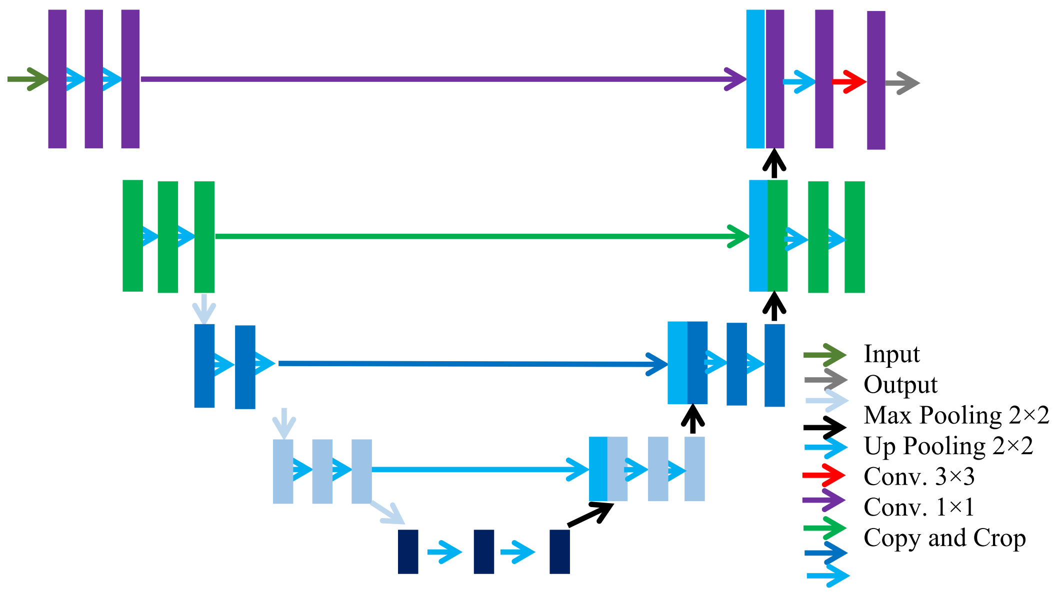

Figure 8: Neural Network Architecture in Proposed Approaches

From a 572×572×1 grayscale input image, the U-Net network produces a 388×388×2 binary segmentation map. Due to the lack of padding, a size difference is generated between the input and output. The input size is preserved using padding. Along the shrinking route, the input image's channels grow as its height and width shrink. Thanks to the raised channels, the network can capture high-level characteristics throughout the transfer process. The last convolution phase that generates a 30x30x1024 feature map is the limiting factor. The extending path restores the image's original size after deleting the bottleneck feature map. The upsampling layers improve the spatial resolution of the feature map while reducing the number of channels. The decoder layers use the shrinking path skip connections to find and improve picture elements. Lastly, items or classes in the input image are represented by each output pixel. The end result is a binary segmentation map that includes both background and foreground pixels. The levels of the proposed methods are listed in Table 5.

Table 5: Summarizes Tire Types and their Description that Used in the Proposed Approaches

Tire TYPE	Definition
Input Layer	Receives the input image as a tensor.
Contracting Path	Down samples the input image to extract high-level features.

In the proposed system, U-Net can perform regression. It is used for image classification, but the convolutional layer can extract features from images to predict continuous variables. To adapt U-Net to regression, some modifications are required.

1 Last layer replacement: The original U-Net contains a fully connected last layer with 1000 outputs to classify 1000 categories. In regression, this layer needs to be replaced with a single output neuron to predict continuous variables.
2 Customized loss function: Regression tasks use MSE or L1 loss function instead of cross-entropy for classification. The expected and actual values' average difference is measured.
3 Fine-tune the network: Regression tasks with transfer learning can start from a pre-trained U-Net. This requires freezing the earlier layers and adjusting the convolutional layer's pre-trained weights. This adapts the network to regression tasks by utilizing its feature extraction capabilities.

Automated systems depend on precise lung cancer diagnoses derived from CT scans. This study introduces U-Net, a deep learning architecture specifically engineered to detect lung cancer in (CT) images. U-Net is appropriate for automatic lung cancer diagnosis in CT images owing to its precise segmentation capabilities that preserve contextual information. The semantics of U-Net segmentation is a crucial aspect that aids in identifying the boundaries of nodules within the lung. U-Net enables accurate measurement of tumor size and morphology, which is essential for diagnosis and therapy planning. The precise characteristics of nodules are a significant parameter to identify lung cancer. U-Net is exceptionally proficient in this regard. The purpose of employing this filter is to attain equilibrium in grayscale photographs by lightening darker regions and darkening lighter regions in a harmonious fashion. These filters were selected based on research of their functionality and their significant influence on outcomes. They were adopted following extensive experimentation, leading to the conclusion that this filter combination produces promising outcomes and significantly modifies the findings. The impact of the processing procedure, both with and without filters, was illustrated to assess their efficacy. Upon preparing the preliminary data, it is partitioned into two subsets which a test and a training set. The k-fold will be employed, involving five experiments. This strategy was implemented because to its enhanced accuracy and proportionality relative to the database size.

8 Evolution and Desiccations the Result

The suggested methodology assesses outcomes through a confusion matrix, a tabular representation that succinctly encapsulates the efficacy of a machine learning model on a designated test dataset. This method visually represents the number of correct and incorrect predictions made by the model. They are often utilized to assess the effectiveness of classification algorithms designed to predict the categorization of each input instance. The matrix represents the frequency of the model's presence in the test data. The following paragraph clarifies the four elements of the confusion matrix, which are A True Positive occurs when the model correctly identifies a positive data item. A real negative occurs when the model correctly identifies a negative data item. False positives denote erroneous predictions of positive data points by the model. False Negatives denote erroneous predictions of negative data points by the model (Abood & AL-Jibory, 2023). The confusion matrix provides essential measures to evaluate system efficiency, which differ according to the four partitions illustrated below.

- Precision: This is the percentage of the group data that the classifier identifies as belonging to the positive class that is considered accurate, as shown in the accuracy equation 2 .

$$\text{Precision} = \mathrm{TP}/(\mathrm{TP} + \mathrm{FP}) \ \ldots\ldots\ldots\ldots..(2)$$

- Recall: A measure of how accurately a classification system predicts the number of positive cases. Based on Formula 3 .

$$\text{Recall(r)} = \mathrm{TP}/(\mathrm{TP} + \mathrm{FN}) \ \ldots\ldots\ \ldots\ldots.(3)$$

- F1-Score: Precision and retention and equation flow are represented by Formula 4 Gulsoy & Kablan (2024).

$$\mathrm{F1} = 2rp/(r + p) = (2 \times \mathrm{TP})/(2 \times \mathrm{TP} + \mathrm{FP} + \mathrm{FN}) \ \ldots\ (4)$$

- Accuracy: A measure of how close the result is to the true value or known value. Represented by Formula 5.

$$\text{Precision} = (\mathrm{TP} + \mathrm{TN})/(\mathrm{TP} + \mathrm{FP} + \mathrm{TN} + \mathrm{FN}) \ \ldots\ldots..(5\ )$$

The training and testing process was carried out in four different stages to measure the impact of image processing operations.

In the first stage: The system was trained and test with the presence of the initial image processing operations represented by the filters. The results obtained by the system were very promising, as illustrated in the Table 6 and Figure 9. Figure 10 illustrates about the proposed model with various metric values.

Table 6: Result training model with initial image processing augmentation operations

TP(test set)=201	
FP(test set)=5	
FN(test set)=2	
TN(test set)=128	
Recall(test set)	0.990%
F1(test set)	0.982%
Precision for set test	0.975%
Accuracy for set test	0.980%
Accuracy (training)	0.961%

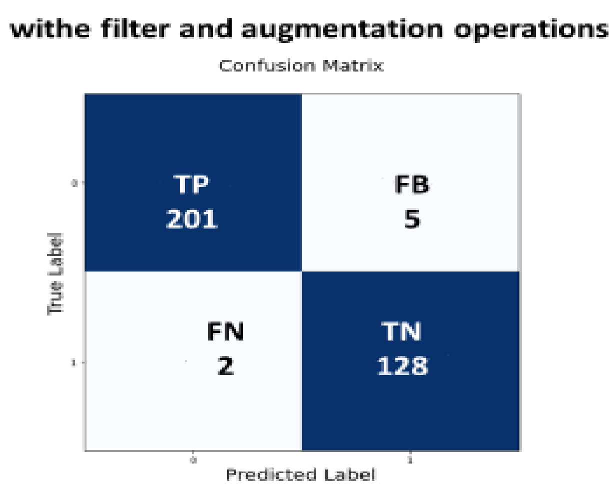

Figure 9: Confusion Matrix with Initial Image Processing and Augmentation Operations

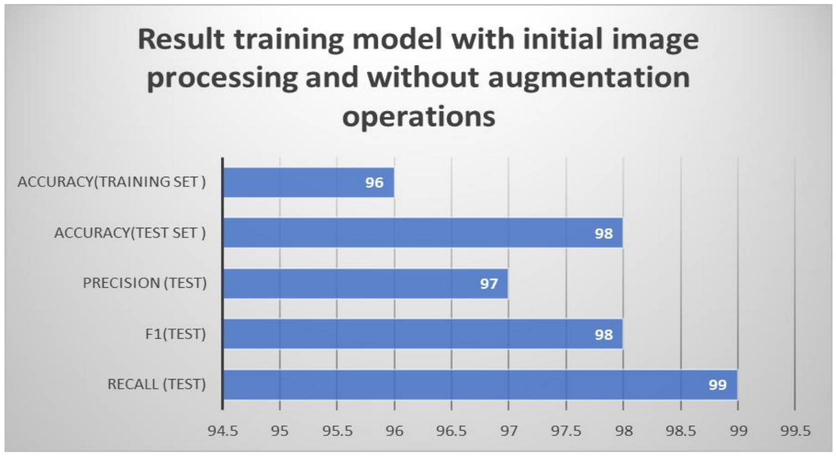

Figure 10: Result of Initial Image Processing and Augmentation Operations

The second stage: The system was trained without the initial image processing operations represented by filters, and the results obtained by the system were relatively lower, as illustrated in the Table 7 and Figure 11. Figure 12 shows the importance of image -preprocessing section with the proposed model without pre-processing section.

Table 7: Result Training Model Without Initial Image Processing and Without Augmentation Operations

TP (test set) = *199*	
FP (test set) = 9	
FN (test set) = 15	
TN (test set) = 15	
Recall (test set)	0.929%
F1(test set)	0.943%
Precision for set test	0.956%
Accuracy for set test	0.899%
Accuracy (training)	0.912%

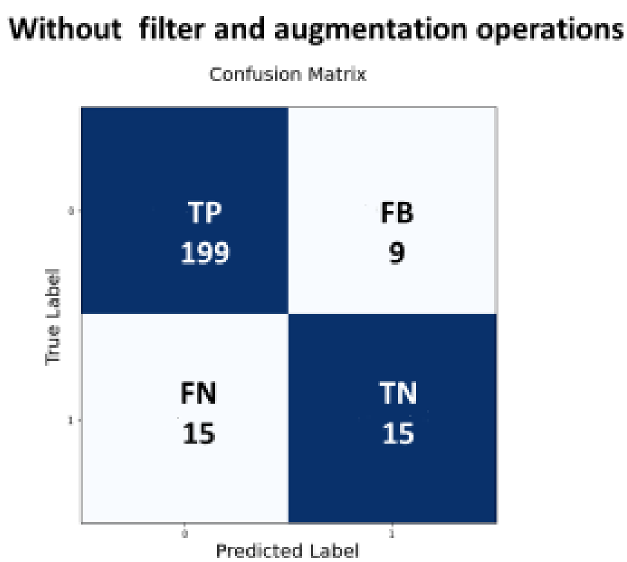

Figure 11: Confusion Matrix Without Initial Image Processing Without Augmentation Operations

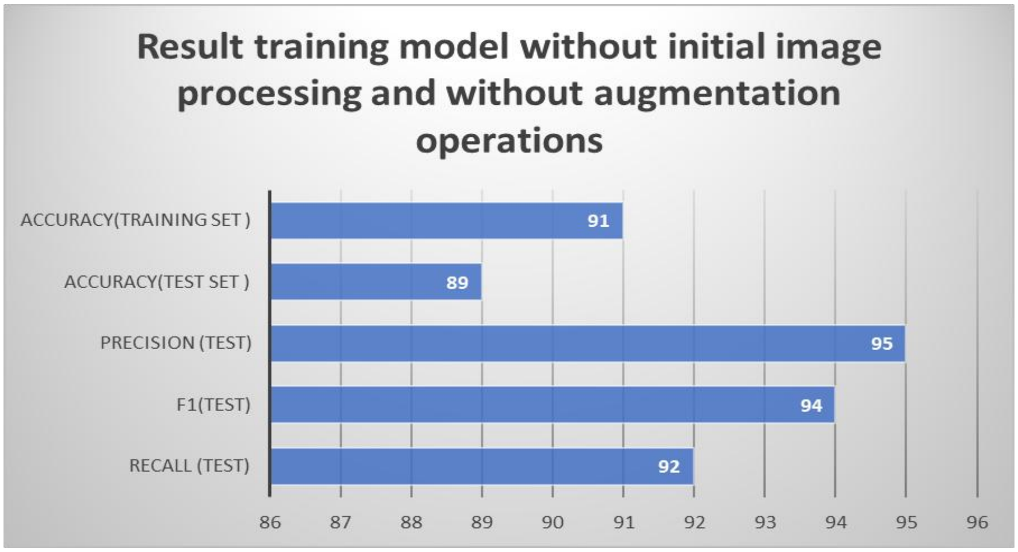

Figure 12: Result of Without Initial Image Processing and Without Augmentation Operations

9 Compared with Previous Studies

Below is a table 8 showing a simple comparison of the results related to previous studies and the proposed approach. The results obtained from the proposed approach were promising. The performance comparison with previous model is illustrated in figure 13.

Table 8: Comparison of the Results with Related to Previous Studies

Re.& year	**Method**	**Dataset**	**Result**
2021 (Kareem et al., 2021)	Filter Segmentation svm	(IQ-OTH/NCCD)	accuracy 89.88%
2021 (AL-Huseiny & Sajit, 2021)	Roi GoogLeNet DNN	(IQ-OTH/NCCD)	**Sensitive** 95.08% **Specificity** 93.7% **Accurse** 94.38%
2022 (Suresha et al., 2022)	EfficientNetB7 and machine learning features are used in the development of the feature fusion. Principal Component Analysis (PCA) is used to further decrease these eEfficnetNetB7 characteristics.	(IQ-OTH/NCCD)	**Precision** 98.4% **Recall** 97% **F-score** 97.7%
2024 (Qadir et al., 2024)	Hybrid-LCSCDM) VGG16 for feature extraction and an XGBoost classifier	(IQ-OTH/NCCD)	**Precision** 0.9863 **Recall** 0.9635 **F-score** 0.9736 **Accuracy** 98.54%

2024 (Gulsoy & Kablan, 2024)	FocalNeXt Augmentation	(IQ-OTH/NCCD)	**Without augmentation** **Sensitivity** (99.78%) **F1-score** (99.56%) **Accuracy** (99.81%) **With augmentation** **Sensitivity** (99.78%) **F1-score** (99.56%) **Accuracy** (98.05%)
2024	MENet (from Xception, InceptionResNetV2, and MobileNetV2 transfer learning-based CNN models)	(IQ-OTH/NCCD) & LIDC-IDRI	**Recall** **92.9%** **F-score** **92.5%** **Accuracy** 95.7%
Proposed approach	CLAHE (DoG) U-NET	(IQ-OTH/NCCD)	initial image processing with augmentation **Recall** (for set test) **= 0.990%** **F1(test set) = 0.982%** **Precision** (for set test) **= 0.975%** **Accuracy** (for set test) **= 0.980%** **Accuracy (training) = 0.961%** training model without initial image processing and without augmentation **Recall (test set) = 0.929%** **F1(test set) = 0.943%** **Precision** (for set test) **= 0.956%** **Accuracy** (for set test) **= 0.899%** **Accuracy (training) = 0.912%**

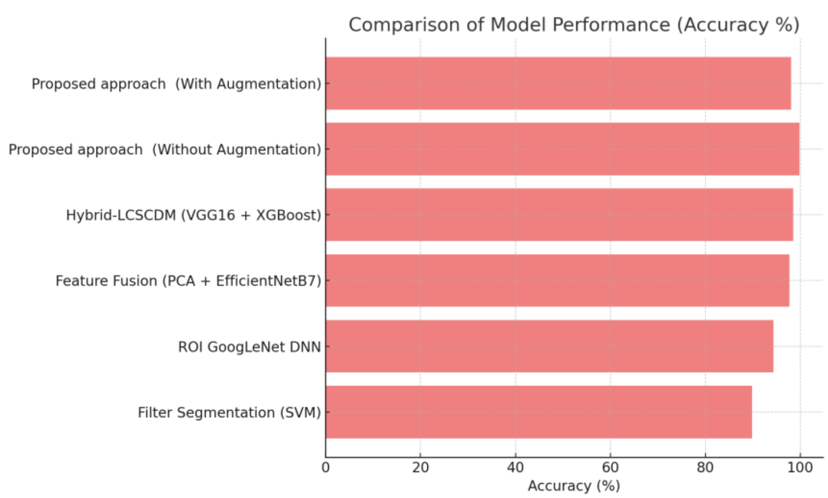

Figure 13: Comparison with Related to Previous Studies

10 Conclusions

This study utilizes U-Net architecture to analyze images from CT for enhanced lung cancer classification. Timely and accurate identification is crucial for the treatment of lung cancer, a predominant cause of cancer-related mortality globally. Conventional diagnostic methods rely on manual interpretation of CT scans, which is labor-intensive and susceptible to errors. Medical imaging encompasses the integration of contemporary image processing methodologies, including filters and their impact on the training of U-Net architecture for lung cancer classification. This study employs deep learning to automatically detect and classify lung cancer from high-resolution CT scans, ensuring precise screening and diagnosis. Automation represents a technological advancement that enhances diagnostic precision and uniformity, mitigating the inconsistencies and resource demands of manual CT analysis. The scientific article measured the influence of initial image processing filter selection through CLAHE and DOG, which improved training results significantly. The augmentation procedure also helped train the suggested approach on hypothetical data the system might encounter but not in the actual data. The pre-trained model U-NET was chosen since it trains deeply with few layers. Measuring the impact of these filters on many pre-trained models might inform future recommendations.

References

[1] Abood, Q. K. (2023). Predicting Age and Gender Using AlexNet. *TEM Journal*, *12*(1).

[2] Al Jibory, F. K., Mohammed, O. A., & Al Tamimi, M. S. H. (2022). Age estimation utilizing deep learning Convolutional Neural Network. *International Journal on Technical and Physical Problems of Engineering*, *14*(4), 219-24.

[3] Al-Huseiny, M. S., & Sajit, A. S. (2021). Transfer learning with GoogLeNet for detection of lung cancer. *Indonesian Journal of Electrical Engineering and computer science*, *22*(2), 1078-1086.

[4] Al-Khafaji, R. S., & Al-Tamimi, M. S. (2022). Vein biometric recognition methods and systems: A review. *Advances in Science and Technology. Research Journal*, *16*(1), 36-46.

[5] Al-Tamimi, M. S. H., & Sulong, G. (2014). Tumor Brain Detection Through MR Images: A Review of Literature. *Journal of Theoretical & Applied Information Technology*, *62*(2).

[6] Al-Tamimi, M. S. H., Sulong, G., & Shuaib, I. L. (2015). Alpha shape theory for 3D visualization and volumetric measurement of brain tumor progression using magnetic resonance images. *Magnetic Resonance Imaging*, *33*(6), 787-803.

[7] Al-Tamimi, M. S., & AL-Khafaji, R. S. (2022). Finger vein recognition based on PCA and fusion convolutional neural network. *International Journal of Nonlinear Analysis and Applications*, *13*(1), 3667-3681.

[8] Aulakh, D., Patil, S., Kumar, M. S., & Bhardwaj, U. (2025). Integration of GIS and Geomorphic Data to Assess the Impact of Landscape Features on River Water Quality. *Natural and Engineering Sciences*, *10*(1), 290-300.

[9] Bhardwaj, S., & Ramesh, T. (2024). Advanced Nanofiber Filters for Sterile Filtration in Biopharmaceutical Processes. *Engineering Perspectives in Filtration and Separation*, 5-7.

[10] Chen, Y., Jiang, G., Li, Y., Tang, Y., Xu, Y., Ding, S., ... & Lu, Y. (2020). A survey on artificial intelligence in chest imaging of COVID-19. *BIO Integration*, *1*(3), 137.

[11] Dodia, S., Annappa, B., & Mahesh, P. A. (2022). Recent advancements in deep learning based lung cancer detection: A systematic review. *Engineering Applications of Artificial Intelligence*, *116*, 105490.

[12] Gayathri, J. L., Abraham, B., Sujarani, M. S., & Ramachandran, S. (2023). A novel CNN framework for the detection of COVID-19 using manta ray optimization and KNN classifier in LUS images. *International Journal of Intelligent Systems and Applications in Engineering*, *11*(2), 55-63.

[13] Gulsoy, T., & Kablan, E. B. (2025). FocalNeXt: A ConvNeXt augmented FocalNet architecture for lung cancer classification from CT-scan images. *Expert Systems With Applications*, *261*, 125553.

[14] Kalavathi, P., & Prasath, V. S. (2016). Methods on skull stripping of MRI head scan images—a review. *Journal of digital imaging*, *29*(3), 365-379.

[15] Kareem, H. F., AL-Husieny, M. S., Mohsen, F. Y., Khalil, E. A., & Hassan, Z. S. (2021). Evaluation of SVM performance in the detection of lung cancer in marked CT scan dataset. *Indonesian Journal of Electrical Engineering and Computer Science*, *21*(3), 1731.

[16] khiled AL-Jibory, F., Younis, M. A., & Al-Tamimi, M. S. (2022). Preparing of ECG Dataset for Biometric ID Identification with Creative Techniques. *TEM Journal*, *11*(4), 1500.

[17] Krishnaiah, P. N. S., & Dayanand Lal, N. (2025). Classification of Lung Diseases Using a Federated Proximal Term-based Two-Layer LSTM with Federated Learning and Blockchain. *Journal of Wireless Mobile Networks, Ubiquitous Computing, and Dependable Applications, 16*(1), 269-288. https://doi.org/10.58346/JOWUA.2025.I1.017.

[18] Kumar, B. S., Karpagavalli, S., Keerthana, K., & Krishnaja, A. (2024). Automatic Segmentation of Colon Cancer Using Sam AI. *Archives for Technical Sciences*, *2*(31), 296-304.

[19] Majumder, S., Gautam, N., Basu, A., Sau, A., Geem, Z. W., & Sarkar, R. (2024). MENet: A Mitscherlich function based ensemble of CNN models to classify lung cancer using CT scans. *Plos one*, *19*(3), e0298527.

[20] Qadir, A. M., Abdalla, P. A., & Abd, D. F. (2024). A Hybrid Lung Cancer Model for Diagnosis and Stage Classification from Computed Tomography Images. *Iraqi Journal for Electrical & Electronic Engineering*, *20*(2).

[21] Raghuram, G. (2024). Synthesis and Characterization of Novel Nanoparticles for Targeted Cancer Therapy. *Clinical Journal for Medicine, Health and Pharmacy*, *2*(4), 21-30.

[22] Seibert, J. A., & Boone, J. M. (2005). X-ray imaging physics for nuclear medicine technologists. Part 2: X-ray interactions and image formation. *Journal of nuclear medicine technology*, *33*(1), 3-18.

[23] Setiawan, A. W., Mengko, T. R., Santoso, O. S., & Suksmono, A. B. (2013, June). Color retinal image enhancement using CLAHE. In *International conference on ICT for smart society* (pp. 1-3). IEEE.

[24] Sharma, A., & Iyer, R. (2023). AI-powered Medical Coding: Improving Accuracy and Efficiency in Health Data Classification. *Global Journal of Medical Terminology Research and Informatics*, *1*(1), 1-4.

[25] Suresha, R., & Devika, K. M. (2022, October). Support vector machine classifier based lung cancer recognition: a fusion approach. In *2022 international conference on edge computing and applications (ICECAA)* (pp. 1-8). IEEE.

[26] Wang, L. (2022). Deep learning techniques to diagnose lung cancer. *Cancers*, *14*(22), 5569.

[27] Zhang, C., Sun, X., Dang, K., Li, K., Guo, X. W., Chang, J., ... & Zhong, W. Z. (2019). Toward an expert level of lung cancer detection and classification using a deep convolutional neural network. *The oncologist*, *24*(9), 1159-1165.

Authors Biography

Mohammed Sabbih Hamoud, Al-Tamimi, Born 16.06.1975 in Basra, Iraq. Bachelor: Computer Science / Computer, College of Science, Al-Fateh University, Tripoli, Libya, 1997; Master: Computer Science / Computer, College of Science, University of Technology and Information, Sana'a, Yemen, 2002; Doctorate: Computer Science / Computer, Multimedia Department, University Technology Malaysia, Johour Bahru, Malaysia, 2016; Last Scientific Position: Assist. Prof. Published 45 papers, 2 theses. Scientific Memberships: Department of Computer Science, College of Science, University of Baghdad, Baghdad, Iraq.

Saadya Fahad Jabbar was born in Baghdad. She earned B.Sc. and M.Sc. degrees in computer science from University of Baghdad and University of Al-Mustansiriyah in 2004 and 2015. Her current position is senior lecturer in information technology at College of Education Ibn Rushd/University of Baghdad. Machine Learning, Natural Language Processing, and Optimization are her research interests.

Ahmed Majid Taha was born in Iraq's Baghdad. In 2007, he earned a Bachelor of Software Engineering from Al-Rafidain University College, Iraq. Later, he began his master's in computer science at UKM and graduated in 2011. In 2014, he began his PhD studies in artificial intelligence at University Tenaga Nasional (UNITEN). Data mining, metaheuristics, algorithms, and machine learning are his research interests. Senior lecturer at College of Biomedical Informatics, University of Information Technology and Communication, Baghdad; member of Soft Computing and Data Mining Center, University Tun Hussein On Malaysia.

Farah Khiled AL-Jibory was born on November 3, 1992, Iraq. She received a Bachelor of Science. Bachelor of Computer Science from Baghdad College of Economic Sciences University in 2014. She received her master's degree in Computer Science from Baghdad University in 2021, Baghdad, Iraq. Currently She is an assistant teacher in the Iraqi Ministry of Education. Her interests are deep learning technologies and branches of artificial intelligence.